

# *HST* Observations and Photoionization Modeling of the LINER Galaxy NGC 1052<sup>1</sup>

J. R. Gabel, F. C. Bruhweiler, D. M. Crenshaw, S. B. Kraemer, and C. L. Miskey

*Institute for Astrophysics and Computational Sciences*

*Department of Physics, The Catholic University of America, Washington, DC 20064*

## ABSTRACT

We present a study of available *Hubble Space Telescope* (*HST*) spectroscopic and imaging observations of the low ionization nuclear emission line region (LINER) galaxy NGC 1052. The WFPC2 imagery clearly differentiates extended nebular H $\alpha$  emission from that of the compact core. Faint Object Spectrograph (FOS) observations provide a full set of optical and UV data (1200-6800 Å). These spectral data sample the innermost region (0."86  $\times$  0."86  $\sim$  82pc  $\times$  82pc) and exclude the extended H $\alpha$  emission seen in the WFPC2 image. The derived emission line fluxes allow a detailed analysis of the physical conditions within the nucleus. The measured flux ratio for H $\alpha$ /H $\beta$ ,  $F_{H\alpha}/F_{H\beta} = 4.53$ , indicates substantial intrinsic reddening,  $E(B-V)=0.42$ , for the nuclear nebular emission. This is the first finding of a large extinction of the nuclear emission line fluxes in NGC 1052. If the central ionizing continuum is assumed to be attenuated by a comparable amount, then the emission line fluxes can be reproduced well by a simple photoionization model using a central power law continuum source with a spectral index of  $\alpha = -1.2$  as deduced from the observed flux distribution. A multi-density, dusty gas gives the best fit to the observed emission line spectrum. Our calculations show that the small contribution from a highly ionized gas observed in NGC 1052 can also be reproduced solely by photoionization modeling. The high gas covering factor determined from our model is consistent with the assumption that our line of sight to the central engine is obscured.

*Subject headings:* galaxies: active — galaxies: individual (NGC 1052)

---

<sup>1</sup>Based on observations made with the NASA/ESA *Hubble Space Telescope*, obtained from the data archive at the Space Telescope Science Institute. STScI is operated by the Association of Universities for Research in Astronomy, Inc. under NASA contract NAS 5-26555.

## 1. Introduction

Low ionization nuclear emission line regions, (LINERs) have been found to occur in nearly 1/3 of all bright, nearby galaxies (Ho et al. 1995). They share many of the emission characteristics of active galactic nuclei (AGN), but are distinguished by their low luminosities and relatively strong, low-ionization emission lines (e.g., [O I]  $\lambda\lambda 6300, 6363$ , [O II]  $\lambda 3727$ , [N II]  $\lambda\lambda 6548, 6584$ , [S II]  $\lambda\lambda 6716, 6731$ ). A recent study by Ho (1999) has demonstrated that the UV – X-ray spectral energy distribution of LINERs is harder than in higher luminosity AGNs. This is consistent with the general trend exhibited in AGNs of decreasing  $\alpha_{ox}$  with decreasing luminosity (Avni & Tananbaum 1982). The physical relation between LINERs and AGNs is unclear. They may be simply the low luminosity extension of the AGN phenomenon, powered by accretion onto a compact object or, alternatively, they may be the result of entirely different mechanisms.

Although central source photoionization appears to be the dominant mechanism powering the nebular emission seen in the high luminosity Seyfert galaxies, it has not been thoroughly tested for galaxies containing LINERs. Competing ionization mechanisms that have been used to successfully explain at least some of the emission characteristics of LINERs include photoionization by hot stars (Terlevich & Melnick 1985, Filippenko & Terlevich 1985), photoionization by non-thermal emission typical of luminous AGN (Ferland & Netzer 1983, Ho et al. 1993) and shock-heating (Heckman 1980, Dopita & Sutherland 1995, Dopita 1996). LINERs might represent a heterogeneous class of objects since the proposed ionization mechanisms can all explain the low apparent luminosity of LINERs. Perhaps more than one of these various mechanisms is at work in the same object.

NGC 1052 is a nearby ( $z=0.0045$ ; de Vaucouleurs et al. 1991) elliptical galaxy (E4) with a strong nuclear emission line spectrum domi-

nated by low ionization features. For example, the [O I]  $\lambda 6300$  and [O II]  $\lambda 3727$  fluxes exceed that of [O III]  $\lambda 5007$ , plus [N II]  $\lambda 6584$ /  $H\alpha > 1$  (Fosbury et al. 1978, Ho et al. 1993, Ho et al. 1997). Fosbury et al. 1978, hereafter F78, showed that the emission line gas is comprised of a luminous central component ( $d \leq 2''$ ) and a diffuse extended region ( $d \sim 20''$ ). Each emission region contributes approximately equally in total Balmer line flux. Furthermore, the extended component emits many of the other prominent optical lines that are observed in the spectrum of the central region, such as [O II]  $\lambda 3727$  and [O III]  $\lambda 5007$  (F78).

The observed optical continuum emission is dominated by the host galaxy, with no clear detection of any underlying non-thermal emission (F78; Fosbury et al. 1981). Radio studies, on the other hand, clearly show it to have both compact and extended continuum emission components. At  $\sim 1.5$  GHz, its radio emission is characterized by a flat, unresolved ( $\leq 1''$ ) core and two weaker lobes extending  $10-15''$  on either side of the compact source (Wrobel 1984). NGC 1052 has been shown to have an IR excess in the  $5-20 \mu\text{m}$  band within the inner  $2''$  of the nucleus (Becklin et al. 1982). A recent analysis of *ROSAT*/*HRI* imagery shows some extended soft X-ray emission, but the low spatial resolution at these energies prevents isolating any compact emission at scales less than  $10''$  (Guainazzi & Antonelli 1999). X-ray observations with *ASCA* indicate a very flat spectrum for the hard X-ray emission (2-10 keV) of NGC 1052 (Guainazzi & Antonelli 1999).

As with LINERs in general, there is much disagreement on the nature of the excitation mechanism responsible for the nuclear activity in NGC 1052. Initial findings have suggested that shock-heating could produce the observed line emission (Koski & Osterbrock 1976; F78). This claim is largely based upon the high electron temperature ( $T \sim 33,000$  K) implied by the strong [O III]  $\lambda 4363$  emission. Furthermore, simple shock excitation models have been shown to

match the prominent optical emission features (Koski & Osterbrock 1976; F78). In an alternate interpretation, Ferland & Netzer (1983), and more recently Ho et al. (1993), have shown that many of the strong emission lines observed in NGC 1052 (and in LINERs in general) could be produced by photoionization from a nonthermal continuum typical of Seyfert galaxies, namely a power law with spectral index,  $\alpha \approx -1.5$ . The major difference in the models between the typically more luminous Seyferts and the LINERs is that the ionizing flux is inferred to be significantly weaker in LINERs. Subsequent detailed photoionization modeling of NGC 1052 by Péquinot (1984), hereafter P84, has shown that many of the optical emission lines, including [O III]  $\lambda 4363$ , could be fit well by photoionization of a multi-density component gas. His study assumed a central photoionizing source consisting of a black body continuum with an X-ray tail extending to higher energies. Recently, a polarimetric study has shown NGC 1052 to have a broad H $\alpha$  emission line component with FWHM  $\sim 5000$  km s $^{-1}$  (Barth et al. 1998). This provides compelling evidence for the presence of a compact object and lends strong support to the non-stellar photoionization hypothesis.

In this paper, we present a detailed analysis of the nuclear activity in the prototypical LINER galaxy NGC 1052. Specifically, we use *Hubble Space Telescope* (HST) observations of NGC 1052 to explore if photoionization represents a viable option in explaining the emission line spectrum in this LINER. In Section 2 we describe the HST imagery and spectroscopic observations used in this study and present our measured emission line fluxes and an analysis of the WFPC2 H $\alpha$  imagery. We examine the possible role of extinction on the emission line fluxes and ionizing continuum. The methodology and results of our photoionization modeling are given in Section 3. In Section 4, we discuss the implications of our results and compare them with previous studies to form a comprehensive picture

of the activity of NGC 1052. Finally, we summarize our results and present our conclusions in Section 5.

## 2. Observations and Emission Line Measurements

### 2.1. FOS Observations

The spectral data used in this study were obtained with the Faint Object Spectrograph aboard the *Hubble Space Telescope* (HST/ FOS) on 1997 January 13. They were retrieved from the Space Telescope Science Institute (STScI) data archives. All observations were of the active nucleus of NGC 1052 through the 0".86-pair square aperture (post-COSTAR), covering 1200-6800 Å. Thus, the aperture sampled the central 82 pc  $\times$  82 pc of the nuclear region of NGC 1052, assuming  $D = 19.6$  Mpc for  $H_0 = 75$  km s $^{-1}$  Mpc $^{-1}$ . The optical and near-UV data were obtained with high resolution gratings giving  $\lambda/\Delta\lambda \sim 1300$ , while the UV spectrum has a lower resolution given by  $\lambda/\Delta\lambda \sim 250$ . The individual spectra are described in Table 1 along with their exposure times, grating settings, and spectral resolutions. Because of a guide-star lock failure, the data may have slightly degraded spectral resolution and sample a slightly larger spatial region than the aperture size would indicate. If the extended regions emit differently than the nucleus, this may have an effect on the observed emission line ratios and absolute fluxes.

Using the maps of Burstein & Heiles (1982), we find a foreground Galactic reddening value of  $E(B-V) = 0.02$  in the direction of NGC 1052. Figure 1 shows the spectrum in the rest frame of NGC 1052, corrected for Galactic extinction using the extinction law of Savage & Mathis (1979).

#### 2.1.1. UV Emission

Examination of the UV spectrum below 2000 Å in Figure 1 shows a weak UV continuum compared to the optical continuum, although, there appears to be a slight rise toward lower wave-

lengths. This UV continuum shows no evidence for recent starburst activity in the nucleus of NGC 1052. Specifically, the common signatures of hot O and B stars, namely broad wind features from C IV  $\lambda 1549$ , Si IV  $\lambda 1400$ , and N V  $\lambda 1240$  and narrower photospheric lines (Neubig & Bruhweiler 1997, 1999), are absent within the low detection limits of the data. Although the results are not definitive, the absence of stellar features is consistent with the UV continuum being produced by a non-thermal compact source. Numerous UV emission lines are detected in the FOS spectrum, compared to the IUE study in which only two lines, C III]  $\lambda 1909$  and C II]  $\lambda 2326$ , were unambiguously measured (Fosbury et al. 1981).

### 2.1.2. Emission-Line Measurements

Visual inspection of the optical and near-UV data at  $\lambda > 2000 \text{ \AA}$  in Figure 1 clearly shows that the host elliptical galaxy dominates the continuum. Strong stellar absorption features are evident and may affect flux measurements of certain emission lines, especially the Balmer lines. In addition, small wavelength variations in the composite stellar spectrum of the host galaxy may mimic emission line features. To remove the spectral contribution of the host galaxy, we have used template spectra of elliptical galaxies from the *HST*/FOS archival database to approximate its integrated stellar spectrum. We selected a proper template spectrum for each of the three optical gratings (G270H, G400H, and G570H) based upon the following criteria:

- 1) We required the prominent absorption features that do not coincide with emission features in NGC 1052 to match those in the host spectrum of NGC 1052 (namely, Mg I  $\lambda 2852$ , Ca II K  $\lambda 3934$ , G Band  $\lambda 4301$ , Fe I  $\lambda 4440$ , Fe I  $\lambda 4532$ , Mg Ib  $\lambda 5176$ , Fe I  $\lambda 5333$ , Ca I/Mg H  $\lambda 5590$ , Na I Doublet  $\lambda 5893$ , and Ca I/ Fe I  $\lambda 6161$ ; Pritchett & van den Bergh 1976, Crenshaw & Peterson 1985);
- 2) We required the overall galactic flux distribution to be similar to that in NGC 1052.

The template spectra were then scaled in magnitude, so that the strengths of the absorption features matched that of NGC 1052, and subtracted from it. Our template spectra are listed in Table 1 and plotted with the corresponding spectra of NGC 1052 in Figure 1. Since there is very little stellar contribution to the UV in elliptical galaxies and no evidence for hot stars in NGC 1052, no template was used for the G160L grating.

We then measured the emission line fluxes using the subtracted spectrum corrected for Galactic extinction. Flux ratios relative to  $H\beta$  are given in Table 2. To measure the line fluxes, uncontaminated continuum regions were selected on either side of the features to be measured. A linear fit was made to the continuum underlying the emission features and the lines were extracted. In several cases, it was difficult to distinguish between real emission lines and artifacts remaining from our attempt to remove the underlying spectrum of the host galaxy. This is most notable in the He II  $\lambda 4686$  emission. In Table 2, we have indicated where these uncertainties are large. The emission line widths are broader than typically observed in the narrow line regions of AGN, corresponding to a range of velocities between  $900 \text{ km s}^{-1} \leq \text{FWHM} \leq 1100 \text{ km s}^{-1}$  (by comparison, the instrumental resolution for the high dispersion gratings is  $\text{FWHM} \sim 230 \text{ km s}^{-1}$ ).

In several cases, it was necessary to deblend line contributors before accurate emission line fluxes could be derived. In all cases, the spectra were converted to velocity space to preserve the correct line widths. For example,  $H\alpha$  is heavily blended with the [N II]  $\lambda\lambda 6548, 6584$  doublet. To extract the  $H\alpha$  feature, the normalized line profile of  $H\beta$  was used to make a template for both of the [N II] lines, since no broad wings were detected on the  $H\beta$  profile. This technique proved more accurate than fitting with Gaussian profiles because it approximates the actual structure of the emission lines. The [N II] template was created by separating the two profiles according to

their intrinsic transition wavelengths and assuming the flux ratio corresponds to that of their Einstein A-values ( $A_{\lambda 6584}/A_{\lambda 6548}=2.96$ ). The wavelength offset and relative flux of the template were then varied until the residual of the [N II] contribution subtracted from the  $H\alpha$ + [N II] line blend gave the best fit to  $H\alpha$ , namely, a single emission feature on a flat continuum (Figure 2a). Figure 2b shows the resulting  $H\alpha$  fit compared to the  $H\beta$  velocity profile and demonstrates the reliability of this technique.

Several other line blends were treated using the same technique. It is important to deblend and provide accurate flux ratios for the [S II]  $\lambda\lambda 6716, 6731$  lines because they provide a low density constraint for the emission line region. To fit them,  $H\beta$  profiles were centered at the intrinsic wavelengths of the two [S II] lines. The flux ratio was varied until residuals were minimized. For line blends of other hydrogen lines, namely  $H\gamma$ + [O III]  $\lambda 4363$  and  $H\epsilon$ + [Ne III]  $\lambda 3967$ , the  $H\beta$  profile was used as a template for the Balmer line since it will have an identical intrinsic shape. All lines which required deblending are noted in Table 2.

### 2.1.3. Uncertainties

The primary sources of uncertainty are continuum placement in extracting emission lines and the approximations associated with the deblending procedure. For the first case, the uncertainty depends on the strength of the emission line relative to the noise of the data and the existence of host galaxy features. We experimented with continuum levels for lines of different strengths. For the optical and near-UV data, where the host galaxy is dominant but spectral resolution is high, this leads to an estimate of the uncertainty for “strong” lines of  $\pm 5\%$  (defined as having  $F \geq F_{H\beta}$ ), for “moderate strength” lines  $\pm 10\%$  ( $0.2 \times F_{H\beta} < F < F_{H\beta}$ ), and for “weak” lines  $\pm 20\%$  ( $F \leq 0.2 \times F_{H\beta}$ ). For wavelengths below  $\sim 2000 \text{ \AA}$ , there is much less contribution from the host galaxy, however, the signal-

to-noise ratio is significantly deteriorated. Consequently, we find flux uncertainties of the moderate strength lines to be  $\pm 20\%$  and the weak lines to be  $\pm 30\%$ , for wavelengths below  $2000 \text{ \AA}$ .

Additional uncertainties are introduced for lines that require deblending. To reliably estimate this uncertainty, the flux of the residual associated with the [N II]  $\lambda 6584$  line (see Figure 2a) was measured and shown to be  $\pm 10\%$  of the measured flux for the line. This represents an upper limit to the general deblending uncertainty because it was the largest relative residual of all procedures. These two uncertainties were then added in quadrature to obtain the total error for the measured line ratios. The total uncertainty estimate for each emission line is listed in Table 2.

### 2.1.4. Reddening

To estimate the internal reddening of NGC 1052, we compared our measured  $H\alpha/H\beta$  flux ratio ( $F_{H\alpha}/F_{H\beta} = 4.53$ , corrected for Galactic extinction) to an assumed intrinsic ratio  $(H\alpha/H\beta)_I$ . For  $N_e = 10^4 \text{ cm}^{-3}$  and  $T_e = 10,000 \text{ K}$  and assuming case B recombination,  $(H\alpha/H\beta)_I = 2.86$ , which is consistent with the typical ratio determined for AGN (Osterbrock 1989). Using the extinction curve of Savage & Mathis (1979), this implies a reddening of  $E(B-V) = 0.42 \pm .20$ , where the uncertainty was derived from the errors associated with the  $H\alpha$  and  $H\beta$  flux measurements. The deduced intrinsic line ratios are listed in Table 2. Uncertainties were estimated from propagation of errors associated with the reddening and observed flux ratios. Since all previous studies of NGC 1052 determined negligible internal reddening, it is important to examine this issue in more detail (Koski & Osterbrock 1976; F78; Fosbury et al. 1981; Ho et al. 1993; Ho et al. 1997).

The intrinsic He II  $\lambda 1640$ /He II  $\lambda 4686$  ratio is theoretically a better measure of reddening than  $H\alpha/H\beta$  because of the large span in wavelength between the two lines (Kraemer et al. 1994). However, the large flux uncertainties associated

with the He II lines greatly diminish the usefulness of this diagnostic for our data set. Yet, we can still use it as a check on our reddening deduced from the Balmer line ratio. We assume an intrinsic ratio of  $(\text{He II } \lambda 1640/\text{He II } \lambda 4686)_I = 6.6$ , corresponding to  $N_e = 10^4 \text{ cm}^{-3}$  and  $T_e = 10,000^\circ \text{ K}$  (Seaton 1978). This is consistent with the dereddened ratio of  $\text{He II } \lambda 1640/\text{He II } \lambda 4686 \geq 4.2$  considering the large uncertainties associated with these line fluxes (Table 2).

We can also use the relative flux ratios of the higher order hydrogen Balmer lines beyond  $H\beta$  as a consistency check. A comparison of the dereddened Balmer ratios with their intrinsic values is given in Table 3 (Osterbrock 1989). They are seen to be consistent within the quoted uncertainties.

The colors of the host galaxy of NGC 1052,  $B-V = 0.91$ ,  $U-B = 0.42$ , are in accord with typical colors found in normal elliptical galaxies of similar Hubble type, E4 (F78). Thus, the large extinction found above is not consistent if applied to the entire galaxy. If the implied reddening is correct, it suggests that dust is localized to the nuclear region of NGC 1052. There is evidence which supports this. The B-R and B-I images of Carter et al. (1983) and B-R image of Davies et al. (1986) clearly show a diffuse dust lane extending out from the central region to about  $20''$ . Furthermore, the IR measurements of Becklin et al. (1982) indicate a large IR excess between 5-20  $\mu\text{m}$  confined within  $2''$  of the nucleus. The strength of the IR flux at these wavelengths is not consistent with stellar radiation emanating from cool stars and may be thermal radiation from heated dust.

## 2.2. $H\alpha$ Imagery

Images of the nuclear region of NGC 1052 were taken with WFPC2/*HST* using the F658N filter on 1996 June 16. These data were obtained from the STScI data archives. This filter isolates any extended  $H\alpha$  emission. In Figure 4, we have combined two exposures (with 800 and 900 s

exposure times) and removed cosmic ray events. The size of the aperture used for the FOS observations is shown over the bright emission core for reference, although the precise position of the aperture is uncertain due to the guide star lock failure. Strong filamentary nebular  $H\alpha$  emission is seen to extend about  $1''$  around the compact nucleus, with a more diffuse halo extending to further distances. At a position angle of  $\sim 235^\circ$  is a narrow filament of  $H\alpha$  emission. This is compared to the radio jet/lobe observed by Wrobel et al. (1984) at 1.5 GHz which is centered at a position angle of  $\sim 275^\circ$ .

## 3. Photoionization Models

The purpose of the following analysis is to determine if the emission in the compact nuclear region of NGC 1052 is consistent with photoionization by a simple non-thermal continuum, characteristic of AGNs. We seek the simplest model, making the fewest number of assumptions, that gives a satisfactory fit to the dereddened intrinsic emission line spectrum. Discrepancies between our model results and the observed spectrum then provide further insight into the actual physical conditions in NGC 1052.

Photoionization models were computed using Version 90 of the computer code CLOUDY (Ferland 1996). These models were parameterized by the gas density  $n_H$ , continuum shape, and ionization parameter

$$U = \frac{Q}{4\pi R^2 n_H c}$$

where  $Q$  is the number of hydrogen ionizing photons  $\text{s}^{-1}$  and  $R$  the distance from the inner face of the cloud to the central continuum source. When a good fit was achieved, observational constraints on the ionizing luminosity provided constraints on  $R$ .

We adopted the following idealized properties of the emission line gas. In cases where more than one density component was required, we assumed that each component was photoionized by

unattenuated radiation from the central source. Thus we assume, *a priori*, relatively small covering factors for any inner gas components. Physically, this corresponds to a clumpy gas composed of radiation bounded clouds. We assume that the observed radiation is emitted from the “front” faces of the clouds, that is, the side of the clouds facing the central continuum source. Each component was assumed to have constant density. We began by omitting dust grains from the emission line gas, hence, in our initial model, we assume solar abundances and that all reddening occurs external to the line emitting region. Thus, the abundances relative to hydrogen are: He =  $1.00 \times 10^{-1}$ , C =  $3.55 \times 10^{-4}$ , N =  $9.33 \times 10^{-5}$ , O =  $7.41 \times 10^{-4}$ , Ne =  $1.17 \times 10^{-4}$ , Mg =  $3.80 \times 10^{-5}$ , Si =  $3.55 \times 10^{-5}$ , S =  $1.62 \times 10^{-5}$ , and Fe =  $3.24 \times 10^{-5}$  (Grevesse & Anders 1989). The effects of grains mixed with the gas will be treated in a later section.

### 3.1. Choice of Model Parameters:

We adopted a simple power law ionizing continuum parameterized by spectral index  $\alpha$ . Observations in the UV and X-ray were used to constrain its shape (Figure 3). We assumed that the observed UV continuum flux was reddened by the same amount as the emission line fluxes,  $E(B-V) = 0.42$ , as deduced from the  $H\alpha/H\beta$  ratio. This gives a projected intrinsic flux at the Lyman edge of  $F_{1Ryd} \sim 1.9 \times 10^{-27}$  ergs s $^{-1}$  cm $^{-2}$  Hz $^{-1}$ . Results from *ASCA* and *ROSAT* show NGC 1052 to have a rather flat spectrum between 2–6 keV, a steeper continuum between both 6–10 keV and  $\sim 1$ –2 keV, and a flattening at energies below 1 keV (Guainazzi & Antonelli 1999). This indicates that the soft X-ray emission is likely heavily absorbed, which is consistent with the modeling by Weaver et al. (1998). If this absorption is due to a dusty gas, then our previous assumption that the UV continuum is attenuated by a column of dust is justified. We chose the observed *ASCA* flux at 6 keV,  $F_{6keV} = 1.4 \times 10^{-30}$  ergs s $^{-1}$  cm $^{-2}$  Hz $^{-1}$ , as the best estimate of the

intrinsic nuclear X-ray flux, as shown in Figure 3. Interpolating between the estimated intrinsic UV continuum flux at 1 Ryd and the X-ray flux at 6 keV gives  $\alpha = -1.2$  and a total intrinsic luminosity for the ionizing continuum of  $L_{>1Ryd} \sim 2.0 \times 10^{42}$  ergs s $^{-1}$ . We note the large uncertainty in this value due to the uncertainty in the amount of obscuration by dust. Previous studies have indicated that the continuum emission in AGNs is typically not reddened as much as the emission line flux, thus, we may be overestimating the total luminosity (Costero & Osterbrock 1977).

In Figure 3 we have plotted the spectral energy distribution of the continuum emission from the radio through hard X-ray energies of the central point source. In each energy band, we have plotted only the emission that cannot be spatially resolved. Data for both the observed and reddening corrected UV continuum are included, illustrating the large effect that our assumed extinction has on the energetics of the active nucleus.

Simple model calculations using a gas with constant density do not match the intrinsic emission line spectrum of NGC 1052 for any choice of density. One important problem with these models is that they cannot match both the auroral and nebular line fluxes simultaneously. When a low density gas is used,  $n_H \sim 10^{3.5}$  cm $^{-3}$ , the nebular lines are fit well (i.e., [O III]  $\lambda\lambda 5007, 4959$ , [N II]  $\lambda\lambda 6548, 6584$ , [O II]  $\lambda 3727$ , and [S II]  $\lambda\lambda 6716, 6731$ ), but their auroral line counterparts are under estimated, namely [O III]  $\lambda 4363$ , [O II]  $\lambda 2470$ , and [S II]  $\lambda\lambda 4069, 4076$ . For higher densities, the opposite is true. As noted earlier, it was the high temperature implied by the [O III]  $\lambda 4363$ /[O III]  $\lambda\lambda 4959, 5007$  ratio that led to the original interpretation of shock excitation for NGC 1052. Indeed, our [O III] line flux ratio, [O III]  $\lambda 4363$ / [O III]  $\lambda\lambda 4959, 5007 \sim 0.089$ , implies  $T > 100,000$  K in the low density limit (Osterbrock 1989), which is a factor  $\sim 5$  higher than we would expect in the O $^{++}$  zone of a photoion-

ized nebulae. However, choosing the high density that matches this ratio under-estimates the other nebular line fluxes because their critical densities are much lower than that of [O III]  $\lambda\lambda 5007, 4959$ , which have critical density,  $n_c = 6.5 \times 10^5 \text{ cm}^{-3}$ .

The detailed analysis of P84 showed this could be remedied by employing two separate gas components having different densities. In this scenario, the nebular lines overwhelm their auroral counterparts in a low density region where their ratios are determined solely by temperature. Conversely, in a higher density gas the nebular line emissions are suppressed due to collisional de-excitation and, consequently, the auroral line fluxes become a more significant source of cooling. Hence, a density stratification effect is mistaken for an indication of high temperature. Multi-component gases having a range of densities are a common feature in models for LINERs and Seyfert galaxies (Halpern & Steiner 1984; Filippenko 1985; Kraemer et al. 1994, 1998). Since we seek the simplest possible model, our method was to find the fewest number of discrete cloud components that would reproduce the observed emission. Although assuming a small number of distinct isolated gas components might be an oversimplification, it provides insight into the physical conditions and structure of the emission line gas. An alternate approach, the locally optimally emitting cloud model, has also been shown to effectively model the narrow line region emission in AGNs (Ferguson et al. 1997).

Thus, as a first modification to the simple model, we assumed a gas comprised of two density components. Our method was to fit the nebular lines that have very low critical densities ([S II]  $\lambda\lambda 6716, 6731$ , [N II]  $\lambda\lambda 6548, 6584$ , and [O II]  $\lambda 3727$ ) with a low density gas, component 1, and the strongest auroral lines (ie, those of  $S^+$ ,  $O^+$ , and  $O^{+2}$ ) with a higher density gas, component 2. Critical densities of various lines place constraints on the density for each component. If the [O II]  $\lambda 3727$  line is a principal coolant for component 1, the gas den-

sity must not be significantly greater than its critical density of  $n_c = 4500 \text{ cm}^{-3}$  (DeRobertis & Osterbrock 1984). A lower limit on the density for component 1 is obtained from the [S II]  $\lambda\lambda 6716, 6731$  doublet lines. The flux ratio [S II]  $\lambda 6716$ / [S II]  $\lambda 6731 = 1.1$  indicates an electron density  $n_e > 300 \text{ cm}^{-3}$  (Aller 1982). For the high density component, the [O III]  $\lambda 4363$ / [O III]  $\lambda 5007$  ratio implies  $6.5 \times 10^5 \leq n_e \leq 3.3 \times 10^7 \text{ cm}^{-3}$  as determined by the critical densities of the two lines. Additionally, the strong [O I]  $\lambda 6300$  emission indicates  $n_e \leq 1.8 \times 10^6 \text{ cm}^{-3}$  (DeRobertis & Osterbrock 1984).

Since the spectrum of NGC 1052 is dominated by lines of low ionization species, lines emitted by  $S^+$ ,  $N^+$ ,  $O^0$ ,  $O^+$ , and  $C^+$ , a low ionization parameter is required. Figure 1 of Ferland & Netzer (1983), which shows the relationship between various line strengths and the ionization parameter for a low density gas, indicates  $U < 10^{-3.5}$  for component 1. We find that a slightly higher  $U$  is needed for component 2 to sufficiently populate the states responsible for the auroral line emission. Model results using  $n_H = 10^{3.5} \text{ cm}^{-3}$ ,  $U_1 = 10^{-3.8}$  and  $n_H = 10^{6.2} \text{ cm}^{-3}$ ,  $U_2 = 10^{-3.1}$  for components one and two, respectively, are presented in columns 3 and 4 of Table 4. The composite model in column 5 of Table 4 was created by assuming equal contribution from each component to the total observed  $H\beta$  flux.

### 3.2. The Effects of Grains in the Emission Line Gas

Inspection of Table 4 shows that the overall intrinsic emission line spectrum of NGC 1052 is fit very well by our photoionization model, which has employed a minimum of assumptions. Particularly, the strong auroral line fluxes of [O III]  $\lambda 4363$ , [O II]  $\lambda 2470$ , and [S II]  $\lambda\lambda 4069, 4076$  are matched well, as are the [O III]  $\lambda 4363$ /[O III]  $\lambda 5007$  and [O II]  $\lambda 2470$ / [O II]  $\lambda 3727$  ratios, which are often mistakenly used as temperature indicators. However, several of the prominent low ionization features are considerably underpredicted.

For example, the observed [N II]  $\lambda\lambda 6548, 6584$ , [S II]  $\lambda\lambda 6716, 6731$ , and [O I]  $\lambda\lambda 6300, 6363$  line fluxes are matched within a factor of two, but are all somewhat underestimated. The C II]  $\lambda 2326$  fit is even worse.

All of these poorly fit lines emit predominately in the warm partially ionized zones, [S II]  $\lambda\lambda 6716, 6731$  and [N II]  $\lambda\lambda 6548, 6584$  most strongly in component 1 and [O I]  $\lambda\lambda 6300, 6363$  and C II]  $\lambda 2326$  primarily in the high density component 2. The characteristic emission in these regions is likely greatly modified by the presence of dust due to the heavy depletion of important coolants (particularly magnesium and silicon) and an increase in gas temperature caused by the selective removal of photons near the Lyman limit by dust grains. To treat this, we have included grains typical of the Orion Nebula mixed with the emission line gas (Baldwin et al. 1991). We selected this type of grain structure since, of the available data for dust grains, physical conditions in an H II region most closely approximate those of NGC 1052. Constraints on the dust-to-gas ratio in NGC 1052 come from the strengths of the Si III]  $\lambda\lambda 1882, 1892$  and Mg II  $\lambda 2800$  fluxes. The calculated emission of these lines becomes too weak when the full depletion deduced for Orion is used in our models (Ferland 1996: based on results of Baldwin et al. 1991, Rubin et al. 1991, and Osterbrock 1992). Therefore, we assumed half of the depletion and grain abundances, giving the following elemental abundances relative to hydrogen: He =  $9.77 \times 10^{-2}$ , C =  $3.31 \times 10^{-4}$ , N =  $8.13 \times 10^{-5}$ , O =  $5.50 \times 10^{-4}$ , Ne =  $8.51 \times 10^{-5}$ , Mg =  $1.07 \times 10^{-5}$ , Si =  $1.20 \times 10^{-5}$ , S =  $1.29 \times 10^{-5}$ , and Fe =  $1.02 \times 10^{-5}$ .

Model results, using the same parameters as in our previous model are given in Table 5. We have included model predictions of the [Ca II]  $\lambda\lambda 7291, 7324$  lines for both the dusty and solar abundance models in Tables 5 and 4, respectively. Ferland (1993) has shown that the weakness of these lines in the narrow line regions of some AGNs is a good indicator of the presence of grains - a sharp

decrease in their strengths is expected with depletion. Indeed, comparison of the results of our two models demonstrates this. Specifically, the dusty model predicts a decrease in the strength of the lines by a factor of ten. Although the [Ca II] lines lie outside of the spectral region covered by our data, the near infrared spectral data of Diaz et al. (1985) clearly show that their strengths are overpredicted by our dust free model (see their Figure 1). Thus, there is evidence that significant depletion exists in NGC 1052.

Our depletion percentage corresponds to a gas column-to-reddening scaling of roughly  $N_H/E(B-V) = 1 \times 10^{22} \text{ cm}^{-2} \text{ mag}^{-1}$  (Knapp & Kerr 1974). The ionized column densities of our gas components are comparatively small ( $N_{HII} = 3.1 \times 10^{19} \text{ cm}^{-2}$  and  $N_{HII} = 3.6 \times 10^{20} \text{ cm}^{-2}$ , for components 1 and 2, respectively). Thus, most of the reddening occurs in a neutral gas obscuring our line of sight to the emitting regions. If this obscuration is due to gas component 1 of our model,  $n_H = 10^{3.5} \text{ cm}^{-3}$ , a cloud thickness of only  $\sim \frac{1}{2}$  pc is required to produce the observed extinction.

The polarimetry study by Barth et al. (1999) shows that [O I]  $\lambda 6300$  is more polarized than the other “narrow” emission lines between  $\sim 4800$ – $6800 \text{ \AA}$ , with a polarization percentage more than twice as much as any other line. This indicates that [O I]  $\lambda 6300$  may be transmitted through more dust than the other lines. This effect is explained naturally, as in our model, if [O I]  $\lambda 6300$  is emitted predominately in an extended dusty partially ionized zone (PIZ). If we are viewing the line emission primarily from the ionized faces of the gas clouds, then the lines emitted in the “back side” of the gas pass through a much larger dust column before escaping. Our calculations show that the PIZ of component 2, where [O I]  $\lambda 6300$  is most strongly produced, has a much larger column density than the PIZ of component 1. Since this is the region where the [N II]  $\lambda\lambda 6548, 6584$  and [S II]  $\lambda\lambda 6716, 6731$  lines are emitted, this explains why there is much less polarization of these lines than of the [O I]  $\lambda 6300$

line.

### 3.3. Structure of the Emission Line Region

We now turn our attention toward the structure of the emission line region as deduced from our model results. Since we have an estimate of the luminosity of ionizing radiation, we can calculate the radial distances of the different gas components from the putative central engine,  $R_1$  and  $R_2$ , using  $U \propto L_{(\geq 1Ryd)}/R^2$ . This gives  $R_1 \sim 100$  pc and  $R_2 \sim 2$  pc. The deduced location of component 1 lies outside the projected aperture by about a factor of 2, however, the uncertainty in the intrinsic luminosity could account for this discrepancy. Furthermore, if the gas is spherically distributed, then much of it would be projected into the aperture.

The broad widths of the emission lines ( $900 \leq \text{FWHM} \leq 1100 \text{ km s}^{-1}$ ) give clues to the gas dynamics in NGC 1052. We find no correlation between line width and critical density. Thus, since the high and low density components are at very different distances from the putative central massive object, the velocities of the two components cannot be explained as simple circular Keplerian orbits, for which  $v \propto r^{-1/2}$ .

As mentioned earlier, our assumption that the line emitting gas is comprised of distinct components having constant densities is a rough approximation, but qualitatively the higher density gas is seen to be closer to the center of the nucleus. To match the calculated  $H\beta$  luminosity with the observed luminosity, covering factors of  $\epsilon_1 = 0.28$  and  $\epsilon_2 = 0.25$  are required for components 1 and 2, respectively, assuming that each component contributes equally to the total  $H\beta$  emission. Model predictions of  $L_{H\beta}$  for each component are given in Table 5. Since the covering factors for each component were calculated independently of each other, the attenuation of the inner component was not treated and hence  $\epsilon_1$  represents a minimum covering factor for the outer component. Therefore, a minimum total

covering factor for NGC 1052 is  $\epsilon_T = 0.53$ , which represents the probability that the line-of-sight to the central continuum is obscured by the emission line gas. This is considerably higher than that determined for the narrow line regions of Seyfert 1 galaxies (Netzer & Laor 1993). Thus, our previous assumption that the central ionizing continuum is occulted by a dusty gas is vindicated. This is consistent with the study by Barth et al. (1998) which concluded that many LINERs may have bright compact UV sources that are obscured by dust.

### 3.4. The High Ionization Component

Although the spectrum of NGC 1052 is dominated by low ionization features, there are several high ionization features present, namely, C IV  $\lambda 1549$ , [Ne IV]  $\lambda 2424$ , and [Ne V]  $\lambda 3426$ . As anticipated from our choice of low ionization parameters,  $U_1$  &  $U_2$ , these lines are greatly underestimated. In particular, the predicted C IV  $\lambda 1549$  is  $\sim 4$  times too weak and [Ne IV]  $\lambda 2424$  and [Ne V]  $\lambda 3426$  are underpredicted by a factor of  $\sim 10$ . Imposing the required  $U$  on either of the two gas components would severely degrade our fit to the prominent low ionization features, giving results characteristic of Seyfert galaxies. Indeed, it is this lower ionization that distinguishes LINERs from other active galaxies. Thus, there is an indication that a highly ionized gas component is present in NGC 1052, although its contribution is small.

The critical density of [Ne IV]  $\lambda 2424$  limits  $n_e \leq 3 \times 10^4 \text{ cm}^{-3}$ . However, for a gas with this low density and having a high ionization parameter, the [O III]  $\lambda\lambda 5007, 4959$  lines become the dominant coolants and their fluxes are far over-predicted. We find that an emitting gas that is matter bounded can account for this. For illustrative purposes, we have calculated the emission for a gas without dust grains having  $U_3 = 10^{-1.5}$  and  $n_H = 10^{4.2} \text{ cm}^{-3}$  and a total column density of  $N_H = 10^{21} \text{ cm}^{-2}$ . This corresponds to a distance  $R_3 \sim 3$  pc of the highly ionized gas from

the central continuum source. A very low covering factor of only  $\sim 0.05$  is required to match the observed C IV  $\lambda 1549$  luminosity with this extra component, hence our assumption that all components receive unattenuated continuum radiation remains valid. This simple model for a highly ionized component matches the observed [Ne V]  $\lambda 3426$  emission line very well and the [Ne IV]  $\lambda 2424$  line within a factor of 2. Furthermore, since the emissivity of C IV  $\lambda 1549$  is very high under these conditions, there would be only a small contribution from this component and, therefore, no change in the low ionization line ratios predicted by a three-component model from those listed in Tables 4 & 5.

#### 4. Discussion

We have shown that a simple photoionization model explains the full set of dereddened optical and UV emission lines observed in the FOS data of NGC 1052 quite well. We note that the reddening correction we have applied to the UV continuum is highly uncertain and that this enhanced luminosity is essential in reproducing the line luminosities. Our best fit model employs a dusty emission line gas with a high covering factor. This is consistent with the apparent absorption of the soft X-ray flux observed in the *ROSAT* data, indicating that the line-of-sight toward the AGN is obscured. The flat intrinsic ionizing continuum ( $\alpha = -1.2$ ) that we have deduced for NGC 1052 is in accord with the recent study by Ho (1999) which demonstrated that a sample of LINERs all have a higher X-ray/UV continuum ratio than found in typical high luminosity AGNs.

##### 4.1. Extended Emission Line Region

We examine if the deduced ionizing continuum flux is sufficient to power the extended emission line region (EELR) emission described in F78. They found a diffuse emission line gas extending out to about  $20''$  from the nucleus hav-

ing a total Balmer line flux similar to that observed in the nuclear emission region. Using their flux measurements and assuming that all of the emission line fluxes experience the extinction that we have deduced from our analysis gives  $L_{H\beta} \sim 2.6 \times 10^{40}$  ergs  $s^{-1}$  for the total  $H\beta$  luminosity in the extended plus compact emission components. A simple photon-counting argument (Netzer & Laor 1993) using our deduced continuum shape and Lyman edge flux demonstrates that a covering factor of  $\sim 2$  is required to produce the  $H\beta$  luminosity.

A covering factor greater than unity indicates that if all of the line emission in NGC 1052 (extended + compact) is powered by photoionization from the putative non-thermal continuum, then our view of this continuum must be even more obscured than we have previously deduced. Furthermore, the large covering factor of the inner gas regions calculated in our model suggests that the shape of the ionizing continuum incident upon the extended region would be greatly modified. However, the attenuation of UV continuum photons by the emission line gas in the compact region would result in a much harder SED incident upon the extended gas and a much higher actual covering factor for the EELR is required. An alternate explanation is that the central source emission is beamed in NGC 1052 such that the continuum flux "seen" by the emitting gas in the extended regions is enhanced. Another possibility, is that some process other than photoionization by the central source drives the emission in the EELR, either stellar photoionization or shock excitation. A detailed analysis of the diffuse emission regions is needed to fully test this.

##### 4.2. Effects of the Choice of Extinction Curve

As noted in section 3, one discrepancy in our model is the underestimate of the C II]  $\lambda 2326$  flux by a factor of  $\sim 2$ . The C II]  $\lambda 2326$  emission is strong in a gas with low ionization parameter and

high density. However, calculations show that the Mg II  $\lambda 2800$  flux is far overpredicted using these model conditions. Alternately, C II]  $\lambda 2326$  is produced predominantly in the PIZ of a photoionized gas, suggesting a stronger X-ray continuum would strengthen the feature. However, the [O I]  $\lambda\lambda 6300, 6363$  line fluxes are more sensitive to the high energy flux and are greatly overestimated if the X-ray continuum is enhanced.

A poor choice of the extinction curve may account for this discrepancy. Several studies have shown that the UV dust extinction in extragalactic objects is not represented well by the Galactic Savage & Mathis curve (Fitzpatrick 1985, Calzetti et al. 1994). Often a weaker 2200 Å absorption feature and steeper rise in the far-UV are found. As an *ad hoc* demonstration, we show how the UV line strengths are affected by removing the 2200 Å bump from the extinction curve in Table 6. The [C II]  $\lambda 2326$  and [Ne IV]  $\lambda 2424$  line fluxes are both significantly reduced, illustrating that if an extinction law incorporating a strong 2200 Å feature were erroneously applied, it could lead to a substantial overestimate of the intrinsic strengths of these lines.

## 5. Conclusions

We have analyzed archival *HST*/FOS data of the prototypical LINER galaxy NGC 1052. The aperture sampled the inner  $\sim 82 \text{ pc} \times 82 \text{ pc}$  of the nuclear region, thereby excluding the extended emission region. One important result is that the deduced  $H\alpha/H\beta$  ratio provides evidence for considerable extinction ( $E(B-V) = 0.42$ ) of the emission line fluxes in NGC 1052. Dust appears to be concentrated in or near the nucleus and may also be attenuating the nonthermal continuum of a compact source, which supports the Barth et al. (1998) conclusion that the nuclei of many LINERs are obscured by dust.

From our modeling results, we find that the nuclear emission observed in the inner region of

NGC 1052 is explained well by photoionization from a simple power law continuum having a flat spectral index,  $\alpha = -1.2$ . Moreover, the ionizing continuum is consistent with our deduced reddening and observed flux distribution. This is also consistent with the study by Ho (1999) which showed that a sample of LINERs all have a flat spectral energy distribution in the ionizing continuum.

Most of the dereddened line fluxes are matched by a model having two dusty gas components of different densities, photoionized by a single power law continuum. The appearance of the C IV  $\lambda 1549$ , [Ne IV]  $\lambda 2424$ , and [Ne V]  $\lambda 3426$  lines in the spectrum indicates a third gas component may be present, characterized by a high ionization parameter. The key exception to our good model fit is the prominent C II]  $\lambda 2326$  line, which is underpredicted by a factor of about two. This flux is heavily affected by the strength of the 2200 Å absorption feature. Hence, the C II]  $\lambda 2326$  line would be overestimated if the 2200 Å bump of the Savage & Mathis extinction curve is not applicable to NGC 1052. This would also help explain the underestimate of the [Ne IV]  $\lambda 2424$  flux.

The large widths of the emission lines and lack of correlation between width and critical density suggests non-gravitational motion of the emission line gas.

We conclude that a pure central source photoionization model with the simplest non-thermal continuum (a simple power law) reproduce the emission line fluxes in the inner region of NGC 1052 quite well. Other processes such as shocks or photoionization by stars are not required to produce the observed emission. However, we cannot rule out the possibility that these mechanisms contribute to the extended nebular emission.

This research has made use of the SIMBAD database operated at CDS, Strasbourg, France and of the NASA/IPAC Extragalactic Database (NED) which is operated by the Jet Propulsion

Laboratory, California Institute of Technology, under contract with the National Aeronautics and Space Administration. We also would like to acknowledge support for the research from NASA grants NAG5-3378 to the IACS at The Catholic University of America. Also, facilities of the Laboratory for Astronomy and Solar Physics at NASA/GSFC were used in performing part of the research. Finally, we are grateful to the referee, Gary Ferland, for his instructive comments and suggestions.

## REFERENCES

- Aller, L. H. 1984, *Physics of Thermal Gaseous Nebulae* (Reidel: Dordrecht)
- Avni, Y., & Tananbaum, H. 1982, *ApJ*, 262, L17
- Baldwin, J. A., Ferland, G. J., Martin, P. G., Corbin, M. R., Cota, S. A., Peterson, B. M., Slettebak, A. 1991, *ApJ*, 374, 580
- Barth, A. J, Ho, L. C., Filippenko, A. V., & Sargent, W. L. W. 1998, *ApJ*, 496, 113
- Barth, A. J, Filippenko, A. V., & Moran, E. C. 1999, *ApJ*, 515, 61
- Burstein, D., & Heiles, C. 1982, *AJ*, 87, 1165
- Becklin, E. E., Tokunaga, A. T., & Wynn-Williams, C. G. 1982, *ApJ*, 263, 624
- Calzetti, D. A., Kinney, A. L., Storchi-Bergmann, T. 1994, *ApJ*, 429, 582
- Carter, D., Jorden, P. R., Thorne, D. J., Wall, J. V., & Straede, J. C. 1983, *MNRAS*, 205, 377
- Costero, R., & Osterbrock, D. E. 1977, *ApJ*, 211, 675
- Crenshaw, D. M., & Peterson, B. M. 1985, *ApJ*, 291, 677
- Davies, R. L., & Illingworth, G. D. 1986, *ApJ*, 302, 234
- DeRobertis, M. M., & Osterbrock, D. E. 1984, *ApJ*, 286, 171
- de Vaucouleurs, G., de Vaucouleurs, A., Corwin, H. G. Jr., Buta, R. J., Paturel, G., & Fouque, P. 1991, *Third Reference Catalog of Bright Galaxies* (New York: Springer)
- Diaz, A. I., Pagel, B. E. J., & Terlevich, E. 1985, *MNRAS*, 214, 41
- Dopita, M. A., & Sutherland, R. S. 1995, *ApJ*, 455, 468
- Dopita, M. A. 1996, in *The Physics of LINERs in View of Recent Observations*, ed. M. Eracleous et al. (San Francisco: ASP), p44
- Ferguson, J. W., Korista, K. T., Baldwin, J. A., & Ferland, G. J. 1997, *ApJ*, 487, 122
- Ferland, G. J., Netzer, H. 1983, *ApJ*, 264, 105
- Ferland, G. J. 1993, in *The Nearest Active Galaxies*, ed. J. Beckman, L. Colina, & H. Netzer (Madrid: Consejo Superior de Investigaciones Cientificas), 75
- Ferland, G. J. 1996, *Hazy, A Brief Introduction to Cloudy*, Univ. of Kentucky, Department of Physics and Astronomy Internal Report
- Filippenko, A. V. 1985, *ApJ*, 289, 475
- Filippenko, A. V., & Terlevich, R. 1992, *ApJ*, 397, L79
- Fitzpatrick, E. L. 1985, *ApJ*, 294, 219
- Fosbury, R. A. E., Mebold, U., Goss, W. M. & Dopita, M. A. 1978, *MNRAS*, 183, 549
- Fosbury, R. A. E., Snijders, M. A. J., Boksenberg, A. & Penston, M. V. 1981, *MNRAS*, 197, 235
- Grevesse, N. & Anders, E. 1989, *Cosmic Abundances of Matter AIP Conference Proceedings 183*, ed. Waddington, C. J., (New York: AIP), p1
- Guainazzi, M. & Antonelli, L. A. 1999, *MNRAS*, 304, L15
- Halpern, J. P. & Steiner, J. E. 1983, *ApJ*, 269, L37
- Heckman, T. 1980, *A&A*, 87, 152
- Ho, L. C., Filippenko, A. V., & Sargent, W. L. W. 1993, *ApJ*, 417, 63
- Ho, L. C., Filippenko, A. V., & Sargent, W. L. W. 1995, *ApJS*, 98, 477

- Ho, L. C., Filippenko, A. V., & Sargent, W. L. W. 1997, *ApJS*, 112, 315
- Ho, L. C. 1999, *ApJ*, 516, 672
- Knapp, G. R & Kerr, F. J. 1974, *A&A* 35, 361
- Koski, A. T. & Osterbrock, D. E. 1976, *ApJ*, 203, L49
- Kraemer, S. B., Wu, C.-C., Crenshaw, D. M., & Harrington, P. 1994, *ApJ*, 435, 171
- Kraemer, S. B., Crenshaw, D. M., Filippenko, A. V., & Peterson, B. M. 1998, *ApJ*, 499, 719
- Netzer, H., & Laor, A. 1993, *ApJ*, 404, L51
- Osterbrock, D. E. 1989, *Astrophysics of Gaseous Nebulae and Active Galactic Nuclei*, (Mill Valley: University Science Press)
- Osterbrock, D. E., Tran, H. D., Veilleux, S. 1992, *ApJ*, 389, 305
- Péquignot, D. 1984, *A&A*, 131, 159
- Pritchett, C., van den Bergh, S. 1976, *ApJS*, 34, 101
- Rubin, R. H., Simpson, J. P., Haas, M. R., Erickson, E. F. 1991, *ApJ*, 374, 564
- Savage, B. D., & Mathis, J. S. 1979, *ARA&A*, 17, 73
- Seaton, M. J. 1978, *MNRAS*, 185, 5P
- Smith Neubig, M. & Bruhweiler, F. C. 1997, *AJ*, 114, 1951
- Smith Neubig, M. & Burhwieler, F. C. 1999, *AJ*, in press
- Sparks, W. B., Wall, J. V., Thorne, D. J., Jordan, P. R., Van Breda, I. G., Rudd, P. J., Jorgensen, H. E. 1985, *MNRAS*, 217, 87
- Terlevich, R., & Melnick, J. 1985, *MNRAS*, 213, 841
- van Gorkom, J. H., Knapp, G. R., Raimond, E., Faber, S. M., Gallagher, J. S. 1986, *AJ*, 91, 791
- Weaver, K. A., Wilson, A. S., Henkel, C., & Braatz, J. A. 1999, *ApJ*, 520, 130
- Wrobel, J. M. 1984, *ApJ*, 284, 531

Fig. 1.— FOS spectra of the nucleus of NGC 1052 from 1250 to 6800 Å, corrected for Galactic reddening. The plotted template spectra are scaled to match the absorption features of NGC 1052 and offset in flux for clarity.

Fig. 2.— (2a) Deblending procedure for  $H\alpha + [N II]$ . The solid line is the  $H\alpha + [N II]$  line blend with the host galaxy template removed. The  $[N II] \lambda\lambda 6548, 6584$  emission line template (dot-dashed line) was created from the  $H\beta$  profile and subtracted to give the  $H\alpha$  (dashed line) emission line. (2B) Comparison of the shape of the deblended  $H\alpha$  profile to the  $H\beta$  profile scaled to match in flux.

Fig. 3.— The multiwavelength spectrum of the nucleus of NGC 1052. The radio data (+) are the measurements of the compact emission ( $\leq 1''$ ) by Wrobel et al. 1984. The IR data points (\*) are within  $< 2''$  (Becklin et al. 1982). The observed and dereddened UV continuum data at 1300 Å are from this study,  $\sim 0''.86$  ( $\diamond$ ). *ASCA* and *ROSAT* data ( $\triangle$ ) are from Guianazzi & Antonelli (1999) with a resolution of  $5'$ . It is unclear how much of this X-ray emission is compact. The ionizing continuum used in our photoionization models is shown as the solid line. The dashed line is the attenuated continuum, assuming the central engine is viewed through the high density gas, component 2.

Fig. 4.— WFPC2 F658N image of the inner region of NGC 1052. The size of the FOS  $0''.86$  square aperture is plotted over the compact emission core for reference. North is up in this image.

TABLE 1  
FOS OBSERVATIONS OF NGC 1052

Data Set	Grating	Resolution (Å)	Exposure (s)	Template Galaxy
Y3K80105T	G160L <sup>a</sup>	~6.4 <sup>b</sup>	1390	...
Y3K80106T	G160L		2430	
Y3K80107T	G160L		2430	
Y3K80108T	G270H	~2.1 <sup>c</sup>	2320	NGC 3608
Y3K80109T	G400H	~3.1 <sup>c</sup>	1200	NGC 3608
Y3K8010AT	G570H	~4.4 <sup>c</sup>	890	NGC 5845

<sup>a</sup>G160L spectra coadded, weighted by exposure time

<sup>b</sup> $\lambda/\Delta\lambda\sim 250$

<sup>c</sup> $\lambda/\Delta\lambda\sim 1300$

TABLE 2  
MEASURED AND DEREDDENED EMISSION LINE RATIOS<sup>a</sup>

	E(B-V)=0.02	E(B-V)=0.44
C IV $\lambda$ 1549	0.14 ( $\pm$ 0.04)	0.75 ( $\pm$ 0.64)
He II $\lambda$ 1640	0.16 ( $\pm$ 0.05)	0.80 ( $\pm$ 0.66)
[O III] $\lambda$ 1663	0.07 ( $\pm$ 0.02)	0.35 ( $\pm$ 0.28)
N III] $\lambda$ 1750	0.04 ( $\pm$ 0.01)	0.20 ( $\pm$ 0.16)
Si II + [Ne III] $\lambda$ 1808-1820	0.10 ( $\pm$ 0.03)	
Si III] $\lambda\lambda$ 1882,1892 <sup>b</sup>	0.14 ( $\pm$ 0.05)	0.80 ( $\pm$ 0.71)
C III] $\lambda$ 1909 <sup>b</sup>	0.35 ( $\pm$ 0.08)	2.00 ( $\pm$ 1.73)
N II] $\lambda$ 2140	0.06 ( $\pm$ 0.01)	
C II] $\lambda$ 2326 <sup>c</sup>	0.58 ( $\pm$ 0.08)	3.80 ( $\pm$ 3.51)
[Ne IV] $\lambda$ 2424	0.02 ( $\pm$ 0.01)	0.10 ( $\pm$ 0.09)
[O II] $\lambda$ 2470	0.14 ( $\pm$ 0.03)	0.60 ( $\pm$ 0.43)
Fe II $\lambda$ 2558-2583	0.03 ( $\pm$ 0.01)	
Fe II $\lambda$ 2601-2640	0.14 ( $\pm$ 0.03)	
Fe II $\lambda$ 2660-2684	0.04 ( $\pm$ 0.01)	
Fe II $\lambda$ 2711-2765	0.15 ( $\pm$ 0.03)	
Fe II $\lambda$ 2823-2844	0.04 ( $\pm$ 0.01)	
Mg II $\lambda$ 2800	::0.46 <sup>d</sup>	1.2
He II $\lambda$ 3204	::0.05	::0.08
[Ne V] $\lambda$ 3346	::0.015	::0.03
[Ne V] $\lambda$ 3426	0.07 ( $\pm$ 0.02)	0.11 ( $\pm$ 0.04)
[O II] $\lambda$ 3727	2.77 ( $\pm$ 0.31)	3.98 ( $\pm$ 0.81)
[Ne III] $\lambda$ 3869	0.60 ( $\pm$ 0.08)	0.82 ( $\pm$ 0.16)
[Ne III] $\lambda$ 3967 <sup>b</sup>	0.20 ( $\pm$ 0.03)	0.27 ( $\pm$ 0.05)
H $\epsilon$ $\lambda$ 3970 <sup>b</sup>	0.14 ( $\pm$ 0.03)	0.19 ( $\pm$ 0.05)
[S II] $\lambda\lambda$ 4069,4076	0.68 ( $\pm$ 0.10)	0.88 ( $\pm$ 0.17)
H $\delta$ $\lambda$ 4102	0.24 ( $\pm$ 0.03)	0.31 ( $\pm$ 0.05)
H $\gamma$ $\lambda$ 4340 <sup>b</sup>	0.44 ( $\pm$ 0.08)	0.53 ( $\pm$ 0.11)
[O III] $\lambda$ 4363 <sup>b</sup>	0.27 ( $\pm$ 0.05)	0.32 ( $\pm$ 0.06)
He II $\lambda$ 4686	::0.18	::0.19
H $\beta$ $\lambda$ 4861	1.00 <sup>e</sup>	1.00 <sup>f</sup>
[O III] $\lambda$ 4959	0.91 ( $\pm$ 0.13)	0.88 ( $\pm$ 0.13)
[O III] $\lambda$ 5007	2.85 ( $\pm$ 0.32)	2.72 ( $\pm$ 0.31)
[N I] $\lambda$ 5200	0.23 ( $\pm$ 0.03)	0.21 ( $\pm$ 0.03)
[N II] $\lambda$ 5755	::0.09	::0.07
He I $\lambda$ 5876	::0.14	::0.10
[O I] $\lambda$ 6300	3.32 ( $\pm$ 0.37)	2.22 ( $\pm$ 0.49)
[O I] $\lambda$ 6364	1.13 ( $\pm$ 0.13)	0.74 ( $\pm$ 0.17)
[N II] $\lambda$ 6548 <sup>b</sup>	1.73 ( $\pm$ 0.26)	1.10 ( $\pm$ 0.29)
H $\alpha$ $\lambda$ 6563 <sup>b</sup>	4.53 ( $\pm$ 0.68)	2.86 ( $\pm$ 0.77)
[N II] $\lambda$ 6583 <sup>b</sup>	5.14 ( $\pm$ 0.77)	3.24 ( $\pm$ 0.87)

TABLE 2—*Continued*

	E(B-V)=0.02	E(B-V)=0.44
He I $\lambda 6678$	::0.07	::0.04
[S II] $\lambda 6716^b$	2.56 ( $\pm 0.38$ )	1.57 ( $\pm 0.43$ )
[S II] $\lambda 6731^b$	2.35 ( $\pm 0.35$ )	1.45 ( $\pm 0.40$ )

<sup>a</sup>Relative to  $H\beta$

<sup>b</sup>Line deblending procedure required for flux measurement

<sup>c</sup>Contains [O III]  $\lambda 2321$  and Si II]  $\lambda 2335$  emission

<sup>d</sup>Mg II  $\lambda 2800$  is heavily absorbed; a fit to the doublet with Gaussian features gives  $Mg II \lambda 2800/H\beta = 0.80$

<sup>e</sup> $F_{H\beta} = 2.65(\pm 0.13) \times 10^{-14}$  ergs s<sup>-1</sup> cm<sup>-2</sup>

<sup>f</sup> $F_{H\beta} = 1.1(\pm 0.7) \times 10^{-13}$  ergs s<sup>-1</sup> cm<sup>-2</sup>

TABLE 3  
INTRINSIC AND DEREDDENED BALMER LINE RATIOS<sup>a</sup>

	Intrinsic <sup>b</sup>	Dereddened <sup>c</sup>
H $\alpha$ $\lambda$ 6563	2.86	2.86 ( $\pm$ 0.77)
H $\gamma$ $\lambda$ 4340	0.47	0.53 ( $\pm$ 0.11)
H $\delta$ $\lambda$ 4102	0.26	0.31 ( $\pm$ 0.05)
H $\epsilon$ $\lambda$ 3970	0.16	0.19 ( $\pm$ 0.05)

<sup>a</sup>Relative to H $\beta$

<sup>b</sup>From Osterbrock 1989

<sup>c</sup> $E(B-V)_T = E(B-V)_G + E(B-V)_I = 0.44$

TABLE 4  
LINE RATIOS FROM MODEL WITHOUT DUST<sup>a</sup>

	Observed <sup>b</sup>	Comp 1 <sup>c</sup>	Comp 2 <sup>d</sup>	Composite <sup>e</sup>
C IV $\lambda$ 1549	0.75 ( $\pm$ 0.64)	-	0.28	0.14
He II $\lambda$ 1640	0.80 ( $\pm$ 0.66)	1.09	1.28	1.19
[O III] $\lambda$ 1663	0.35 ( $\pm$ 0.28)	-	0.49	0.25
N III] $\lambda$ 1750	0.20 ( $\pm$ 0.16)	-	0.20	0.10
Si III] $\lambda$ 1882,1892	0.80 ( $\pm$ 0.71)	0.01	1.12	0.57
C III] $\lambda$ 1909	2.00 ( $\pm$ 1.73)	0.21	3.50	1.86
C II] $\lambda$ 2326 <sup>g</sup>	3.80 ( $\pm$ 3.51)	1.00	2.56	1.78
[Ne IV] $\lambda$ 2424	0.10 ( $\pm$ 0.09)	-	0.01	0.01
[O II] $\lambda$ 2470	0.60 ( $\pm$ 0.43)	0.30	1.11	0.71
Mg II $\lambda$ 2800	::1.2	1.77	4.50	3.14
He II $\lambda$ 3204	::0.08	0.07	0.08	0.08
[Ne V] $\lambda$ 3346	::0.03	-	-	<0.01
[Ne V] $\lambda$ 3426	0.11 ( $\pm$ 0.04)	-	-	<0.01
[O II] $\lambda$ 3727	3.98 ( $\pm$ 0.81)	7.07	0.09	3.58
[Ne III] $\lambda$ 3869	0.82 ( $\pm$ 0.16)	0.82	1.92	1.37
[Ne III] $\lambda$ 3967	0.27 ( $\pm$ 0.05)	0.25	0.60	0.43
H $\epsilon$ $\lambda$ 3970	0.19 ( $\pm$ 0.05)	0.17	0.16	0.17
[S II] $\lambda\lambda$ 4069,4076	0.88 ( $\pm$ 0.17)	0.49	0.92	0.71
H $\delta$ $\lambda$ 4102	0.31 ( $\pm$ 0.05)	0.27	0.27	0.27
H $\gamma$ $\lambda$ 4340	0.53 ( $\pm$ 0.11)	0.47	0.47	0.47
[O III] $\lambda$ 4363	0.32 ( $\pm$ 0.06)	-	0.59	0.30
He II $\lambda$ 4686	::0.19	0.12	0.14	0.13
H $\beta$	1.00	1.00	1.00	1.00
[O III] $\lambda$ 4959	0.88 ( $\pm$ 0.13)	0.34	1.72	1.03
[O III] $\lambda$ 5007	2.72 ( $\pm$ 0.32)	0.97	4.98	2.98
[N I] $\lambda$ 5200	0.21 ( $\pm$ 0.03)	0.25	0.01	0.13
[N II] $\lambda$ 5755	::0.07	0.05	0.17	0.11
He I $\lambda$ 5876	::0.10	0.17	0.15	0.16
[O I] $\lambda$ 6300	2.22 ( $\pm$ 0.49)	1.23	2.19	1.71
[O I] $\lambda$ 6364	0.74 ( $\pm$ 0.17)	0.39	0.70	0.55
[N II] $\lambda$ 6548	1.10 ( $\pm$ 0.29)	1.36	0.29	0.83
H $\alpha$ $\lambda$ 6563	2.86 ( $\pm$ 0.77)	2.92	2.96	2.94
[N II] $\lambda$ 6583	3.24 ( $\pm$ 0.87)	4.03	0.85	2.44
He I $\lambda$ 6678	::0.04	0.05	0.03	0.04
[S II] $\lambda$ 6716	1.57 ( $\pm$ 0.43)	1.47	0.06	0.77
[S II] $\lambda$ 6731	1.45 ( $\pm$ 0.40)	2.03	0.14	1.09
[Ca II] $\lambda$ 7291	-	0.61	0.06	0.34
[Ca II] $\lambda$ 7324	-	0.40	0.04	0.22

<sup>a</sup>Relative to H $\beta$

21

<sup>b</sup>Corrected for Galactic and internal reddening, E(B-V)=0.44

<sup>c</sup>U=10<sup>-3.8</sup>, N<sub>H</sub>=10<sup>3.5</sup>

TABLE 5  
BEST-FIT MODEL:INCLUDES DUST GRAINS <sup>a</sup>

	Observed <sup>b</sup>	Comp 1 <sup>c</sup>	Comp 2 <sup>d</sup>	Composite <sup>e</sup>
C IV $\lambda$ 1549	0.75 ( $\pm$ 0.64)	-	0.38	0.19
He II $\lambda$ 1640	0.80 ( $\pm$ 0.66)	0.84	1.28	1.06
[O III] $\lambda$ 1663	0.35 ( $\pm$ 0.28)	0.01	0.53	0.27
N III] $\lambda$ 1750	0.20 ( $\pm$ 0.16)	-	0.25	0.13
Si III] $\lambda\lambda$ 1882,1892	0.80 ( $\pm$ 0.71)	0.02	0.54	0.28
C III] $\lambda$ 1909	2.00 ( $\pm$ 1.73)	0.35	4.53	2.44
C II] $\lambda$ 2326 <sup>g</sup>	3.80 ( $\pm$ 3.51)	1.45	2.86	2.16
[Ne IV] $\lambda$ 2424	0.10 ( $\pm$ 0.09)	-	0.01	0.01
[O II] $\lambda$ 2470	0.60 ( $\pm$ 0.43)	0.36	1.02	0.69
Mg II $\lambda$ 2800	::1.2	0.89	1.16	1.03
He II $\lambda$ 3204	::0.08	0.05	0.08	0.07
[Ne V] $\lambda$ 3346	::0.03	-	-	<0.01
[Ne V] $\lambda$ 3426	0.11 ( $\pm$ 0.04)	-	-	<0.01
[O II] $\lambda$ 3727	3.98 ( $\pm$ 0.81)	7.35	0.09	3.72
[Ne III] $\lambda$ 3869	0.82 ( $\pm$ 0.16)	0.78	1.68	1.23
[Ne III] $\lambda$ 3967	0.27 ( $\pm$ 0.05)	0.23	0.51	0.37
He $\epsilon$ $\lambda$ 3970	0.19 ( $\pm$ 0.05)	0.17	0.16	0.16
[S II] $\lambda\lambda$ 4069,4076	0.88 ( $\pm$ 0.17)	0.55	1.06	0.81
H $\delta$ $\lambda$ 4102	0.31 ( $\pm$ 0.05)	0.26	0.27	0.27
H $\gamma$ $\lambda$ 4340	0.53 ( $\pm$ 0.11)	0.47	0.47	0.47
[O III] $\lambda$ 4363	0.32 ( $\pm$ 0.06)	0.01	0.58	0.30
He II $\lambda$ 4686	::0.19	0.09	0.14	0.12
H $\beta$ <sup>h</sup>	1.00	1.00	1.00	1.00
[O III] $\lambda$ 4959	0.88 ( $\pm$ 0.13)	0.33	1.50	0.92
[O III] $\lambda$ 5007	2.72 ( $\pm$ 0.31)	0.96	4.34	2.45
[N I] $\lambda$ 5200	0.21 ( $\pm$ 0.03)	0.40	0.02	0.21
[N II] $\lambda$ 5755	::0.07	0.06	0.19	0.13
He I $\lambda$ 5876	::0.10	0.16	0.14	0.15
[O I] $\lambda$ 6300	2.22 ( $\pm$ 0.49)	1.40	2.49	1.95
[O I] $\lambda$ 6364	0.74 ( $\pm$ 0.17)	0.45	0.79	0.62
[N II] $\lambda$ 6548	1.10 ( $\pm$ 0.29)	1.44	0.36	0.90
H $\alpha$ $\lambda$ 6563	2.86 ( $\pm$ 0.77)	2.93	2.92	2.93
[N II] $\lambda$ 6583	3.24 ( $\pm$ 0.87)	4.26	1.05	2.66
He I $\lambda$ 6678	::0.04	0.04	0.03	0.04
[S II] $\lambda$ 6716	1.57 ( $\pm$ 0.43)	1.72	0.10	0.91
[S II] $\lambda$ 6731	1.45 ( $\pm$ 0.40)	2.20	0.23	1.22
[Ca II] $\lambda$ 7291	-	0.07	0.01	0.04
[Ca II] $\lambda$ 7324	-	0.04	0.01	0.03

<sup>a</sup>Relative to H $\beta$

<sup>b</sup>Corrected for Galactic and internal reddening, E(B-V)=0.44

<sup>c</sup>U=10<sup>-3.8</sup>, N<sub>H</sub>=10<sup>3.5</sup>

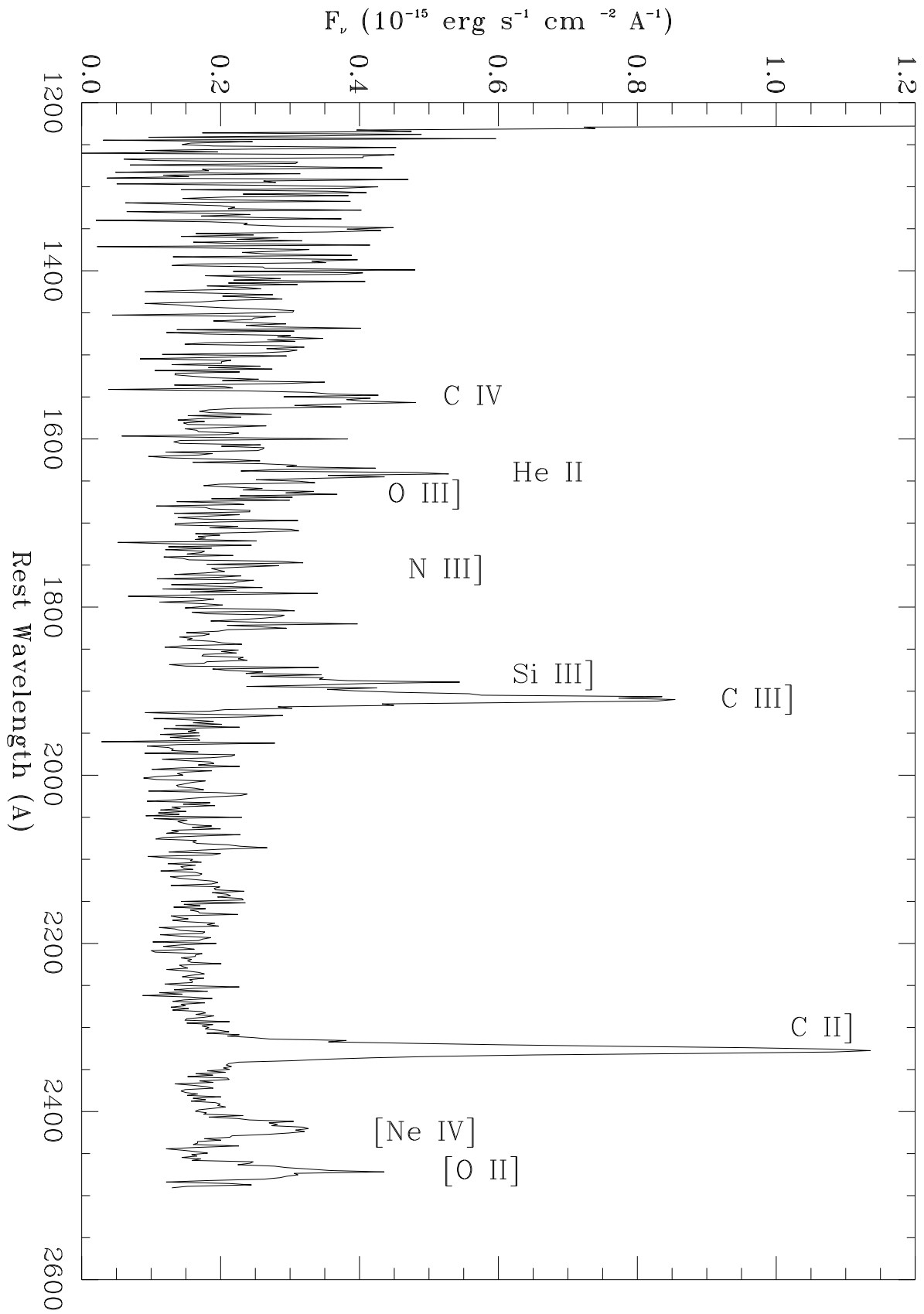
TABLE 6  
THE EFFECT OF THE 2200 Å FEATURE IN THE EXTINCTION CURVE

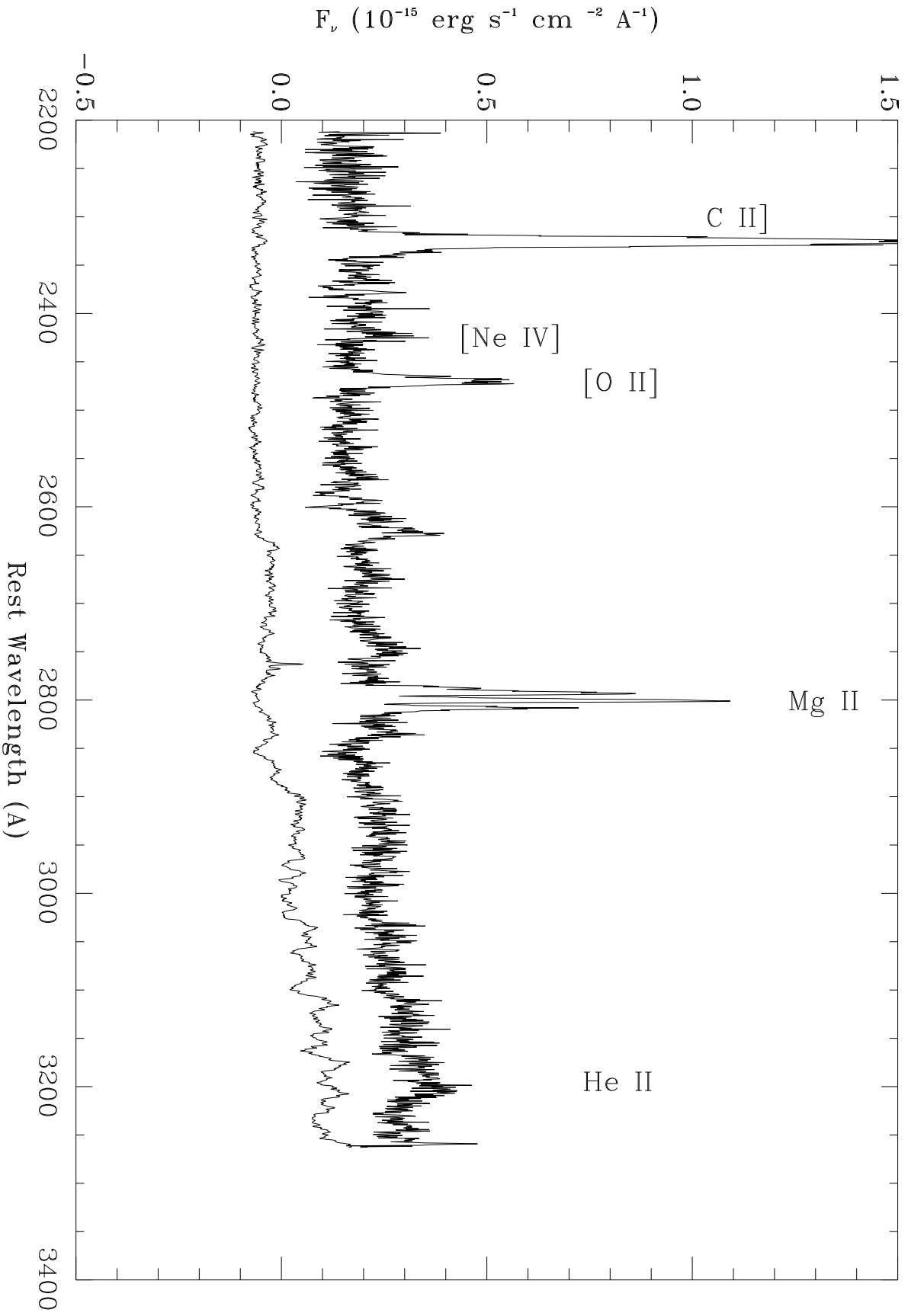
	S & M Curve <sup>a</sup>	Modified S & M Curve, <sup>ab</sup>	Best-Fit Model
C IV λ1549	0.75 (± 0.64)	0.75	0.19
He II λ1640	0.80 (± 0.66)	0.80	1.06
[O III] λ1663	0.35 (± 0.28)	0.35	0.27
N III] λ1750	0.20 (± 0.16)	0.20	0.13
Si III] λλ1882,1892	0.80 (± 0.71)	0.70	0.28
C III] λ1909	2.00 (± 1.73)	1.69	2.44
C II] λ2326 <sup>c</sup>	3.80 (± 3.51)	2.01	2.16
[Ne IV] λ2424	0.10 (± 0.09)	0.07	0.01
[O II] λ2470	0.60 (± 0.43)	0.39	0.69

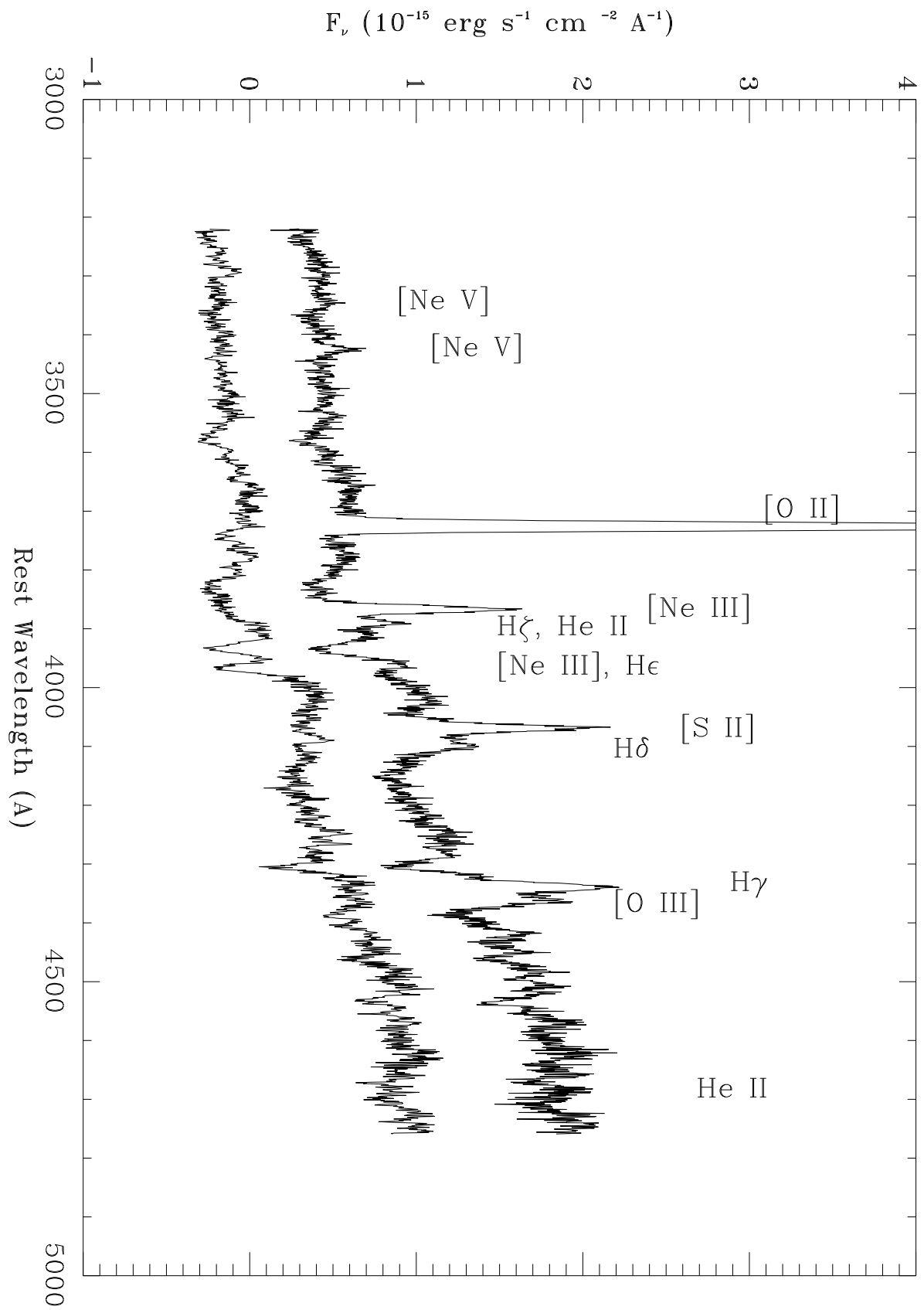
<sup>a</sup> $E(B-V)_T = 0.44$

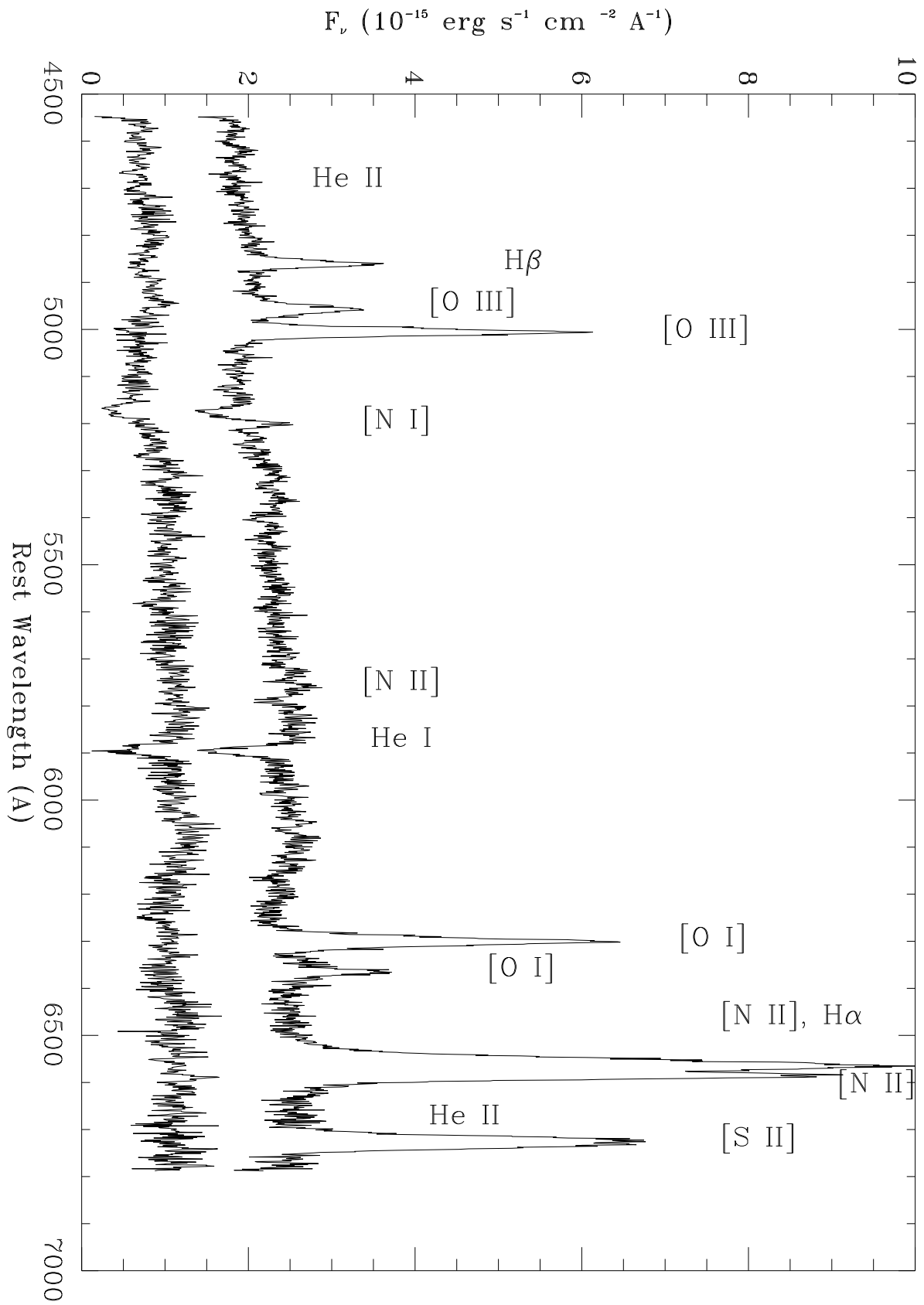
<sup>b</sup>Savage & Mathis extinction curve with 2200 Å feature removed,  $E(B-V)_T = 0.44$

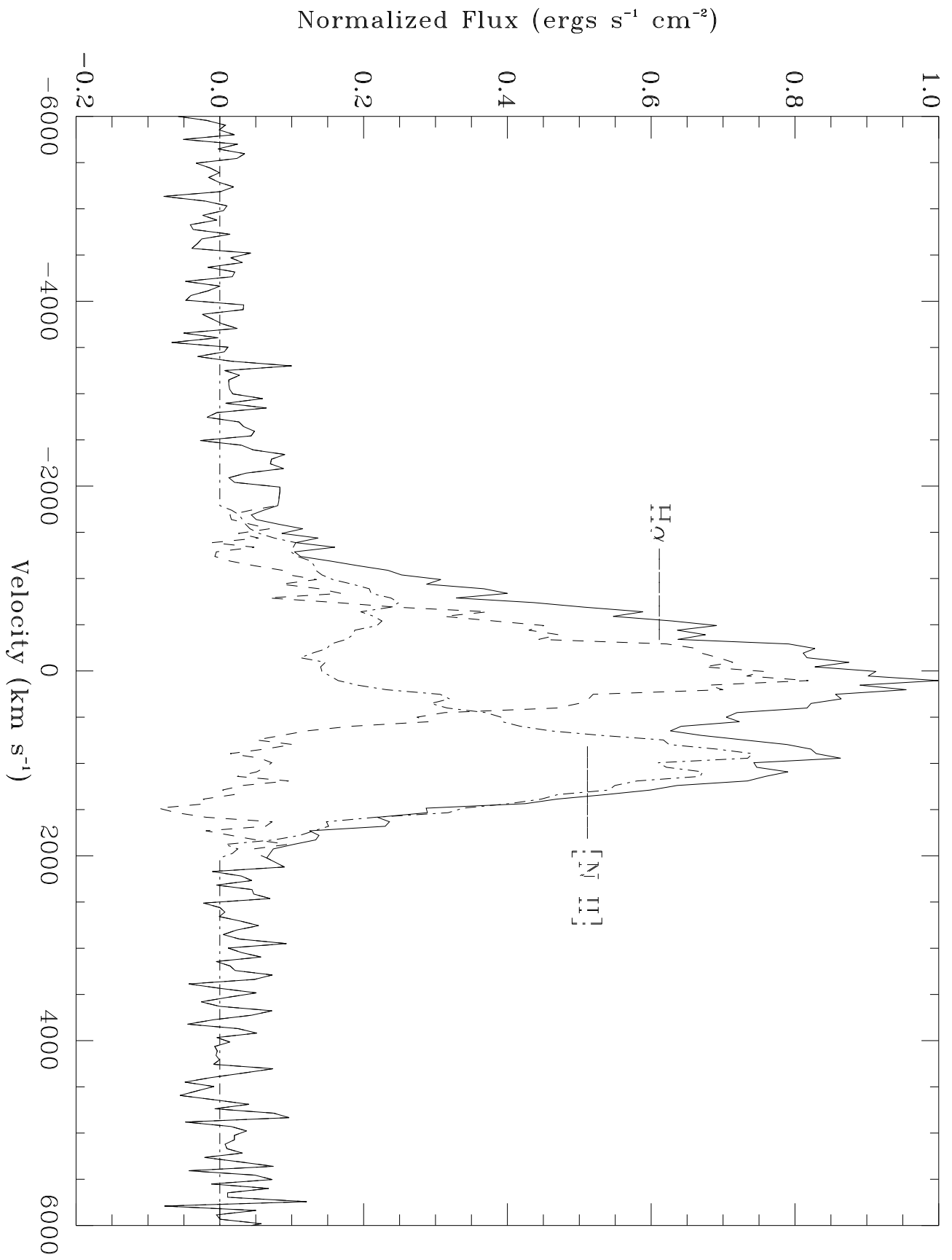
<sup>c</sup>Contains [O III] λ2321 and Si II] λ2335 emission

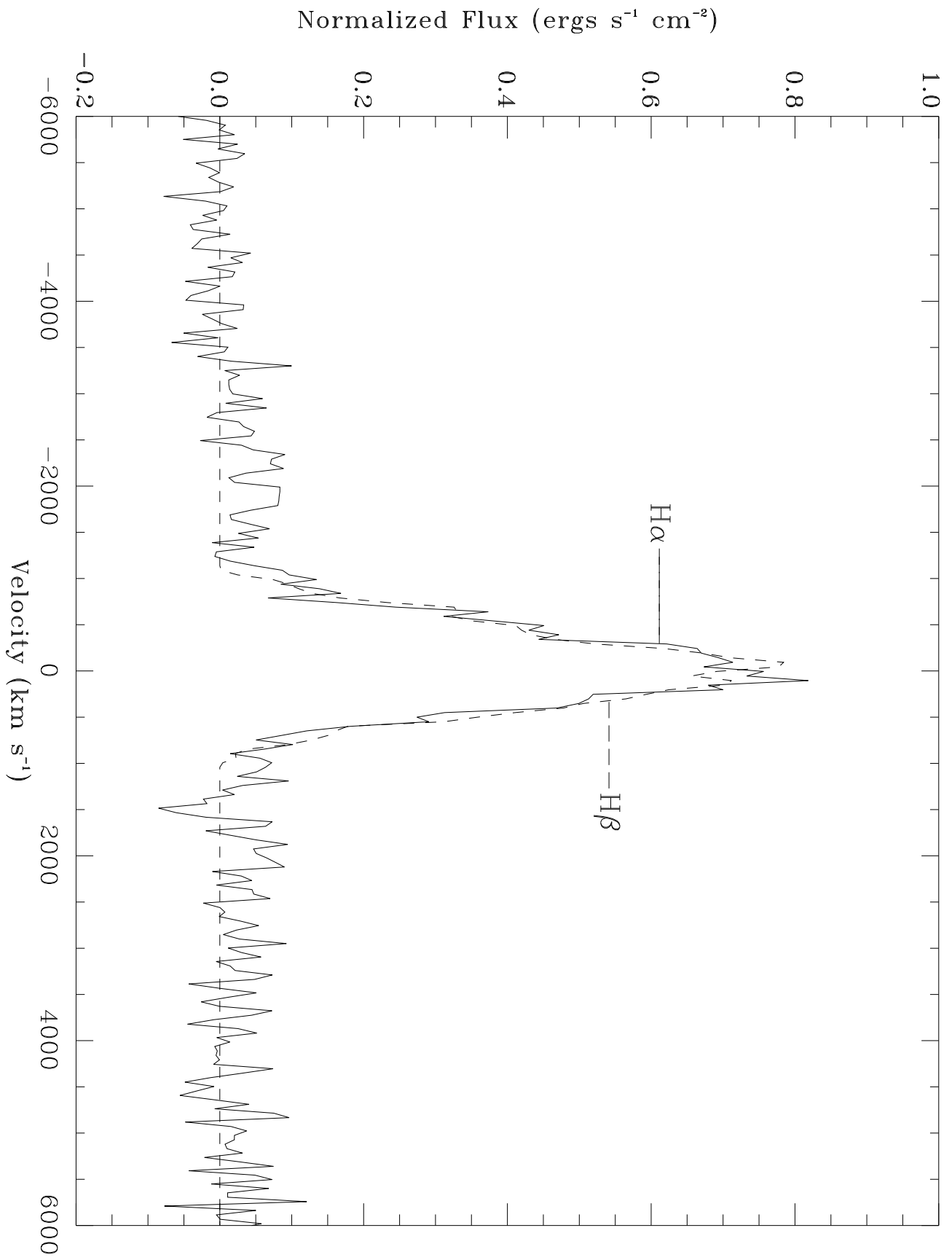


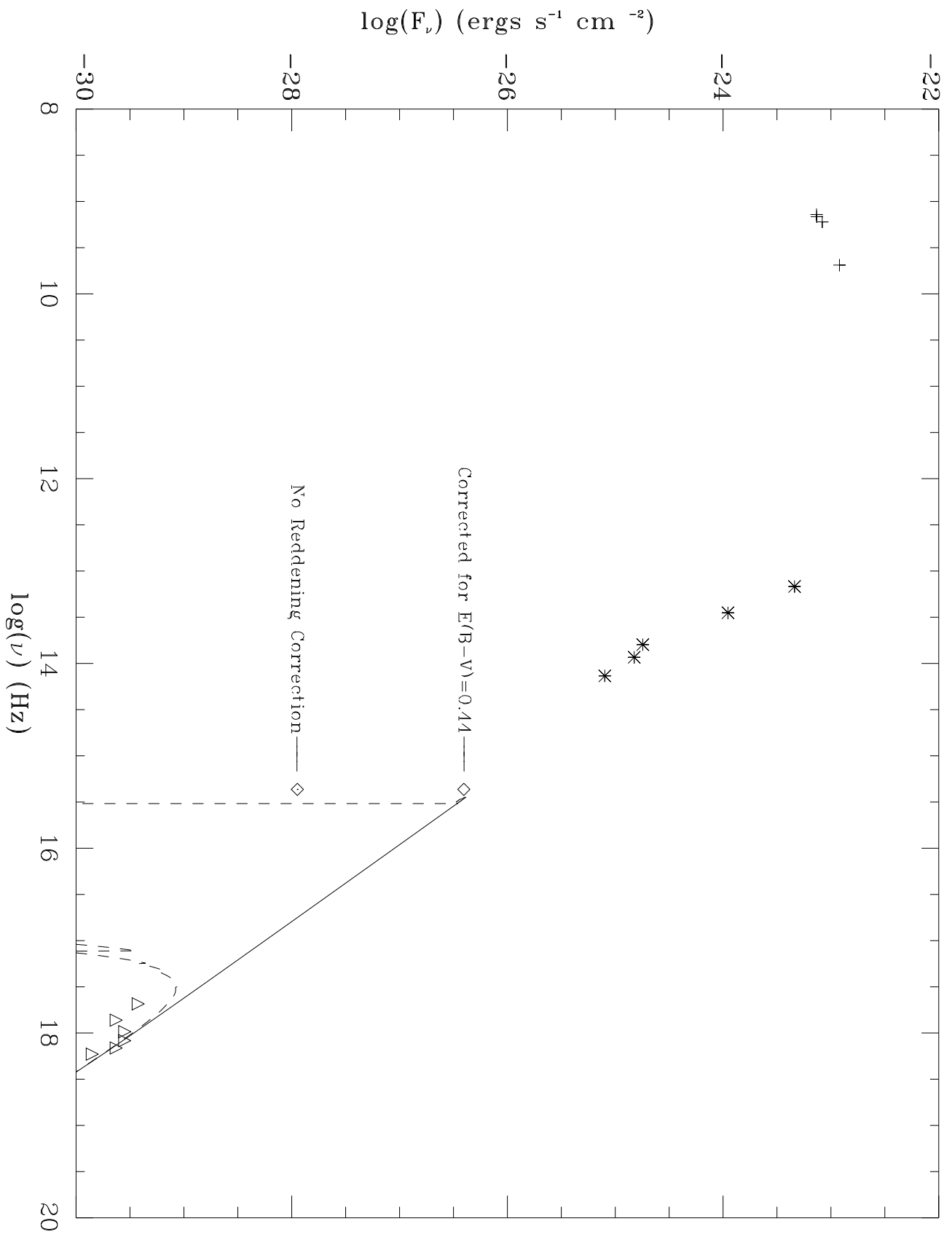












This figure "Fig4.jpg" is available in "jpg" format from:

<http://arxiv.org/ps/astro-ph/0001346v1>